The Ancient Blue Oak Woodlands of California: Longevity and Hydroclimatic History

D. W. Stahle,[*,+] **R. D. Griffin,**[#] **D. M. Meko,**[@] **M. D. Therrell,**[&]
J. R. Edmondson,[*] **M. K. Cleaveland,**[*] **L. N. Stahle,**[**]
D. J. Burnette,[++] **J. T. Abatzoglou,**[##] **K. T. Redmond,**[@@]
M. D. Dettinger,[&&] **and D. R. Cayan**[&&]

[*] Department of Geosciences, University of Arkansas, Fayetteville, Arkansas
[#] Department of Geography, University of Arizona, Tucson, Arizona
[@] Laboratory of Tree-Ring Research, University of Arizona, Tucson, Arizona
[&] Department of Geography, University of Alabama, Tuscaloosa, Alabama
[**] Department of Earth Sciences, Montana State University, Bozeman, Montana
[++] Department of Earth Sciences, University of Memphis, Memphis, Tennessee
[##] Department of Geography, University of Idaho, Moscow, Idaho
[@@] Western Regional Climate Center, Desert Research Institute, Reno, Nevada
[&&] Scripps Institution of Oceanography, U.S. Geological Survey, University of California, San Diego, La Jolla, California

ABSTRACT: Ancient blue oak trees are still widespread across the foothills of the Coast Ranges, Cascades, and Sierra Nevada in California. The most extensive tracts of intact old-growth blue oak woodland appear to survive on rugged and remote terrain in the southern Coast Ranges and on the foothills west and southwest of Mt. Lassen. In the authors' sampling of old-growth stands, most blue oak appear to have recruited to the canopy in the middle to late nineteenth century. The oldest living blue oak tree sampled was over 459 years old, and

[+] Corresponding author address: D. W. Stahle, Department of Geosciences, Ozark Hall 216, University of Arkansas, Fayetteville, AR 72701.

E-mail address: dstahle@uark.edu

several dead blue oak logs had over 500 annual rings. Precipitation sensitive tree-ring chronologies up to 700 years long have been developed from old blue oak trees and logs. Annual ring-width chronologies of blue oak are strongly correlated with cool season precipitation totals, streamflow in the major rivers of California, and the estuarine water quality of San Francisco Bay. A new network of 36 blue oak chronologies records spatial anomalies in growth that arise from latitudinal changes in the mean storm track and location of land-falling atmospheric rivers. These long, climate-sensitive blue oak chronologies have been used to reconstruct hydroclimatic history in California and will help to better understand and manage water resources. The environmental history embedded in blue oak growth chronologies may help justify efforts to conserve these authentic old-growth native woodlands.

1. Introduction

The blue oak (*Quercus douglasii*) ecosystem of California is a mosaic of savanna and woodland that encircles Central Valley on the foothills of the Coast Ranges, Cascades, and Sierra Nevada (Pavlik et al. 1991). These beautiful endemic woodlands constitute one of the largest and most diverse ecosystems in the state (Figure 1), but they have not received a fraction of the attention of California's justly famous conifer forests. Blue oak woodlands have been used for livestock range since European settlement and have increasingly suffered agricultural and urban development. However, blue oak does not produce commercially valuable timber and was not industrially logged for lumber. In spite of past clearing, cordwood cutting, and charcoal operations, old-growth blue oak woodlands with canopy-dominant individual trees from 150 to over 400 years old are still surprisingly widespread in California, particularly on more remote and rugged terrain (Stahle et al. 2001). In fact, the remnant old-growth blue oak ecosystem may be one of the most extensive presettlement woodland cover types left in California. Grazing has altered the native herbaceous layer and has impacted the regeneration dynamics of many remnant blue oak woodlands (Griffin and Muick 1990), but the canopy trees in ancient blue oak forests often predate European settlement and these native woodlands preserve a major component of the eroding biodiversity of California.

Blue oak woodlands form the lower forest border between valley grasslands and midelevation conifer forests where they are frequently exposed to drought and wildfire (Figure 2). Annual growth rings recovered from ancient blue oak trees and fallen logs record an intricate history of drought and wetness spanning the past 300–700 years (Meko et al. 2011). These tree-ring records of precipitation history provide a valuable long-term perspective useful for water resource management and for understanding the natural variability of California climate prior to human influences (Meko et al. 2001; Meko et al. 2011; Stahle et al. 2011).

This article describes tree-ring data from 36 old-growth blue oak woodlands and uses the strong precipitation signal embedded in the annual growth rings to reconstruct cool season precipitation for the North and South Coast Ranges and seasonal salinity levels in San Francisco Bay. The salinity reconstruction is possible

Figure 1. This blue oak woodland is located on private property in Bear Creek Canyon, Tehama County, near the northern limit of the species distribution. The larger trees are in the 150–250-yr age range.

because tree growth, streamflow, and freshwater inflow to the estuary are all controlled by winter precipitation totals in California. These new reconstructions provide multicentury perspectives on the natural variability of California precipitation and estuarine salinity. The salinity estimates suggest that the high salinity extremes witnessed in San Francisco Bay during the severe droughts and freshwater diversions of the 1970s, 1980s, and early 1990s were unmatched over the past 670 years.

2. Blue oak distribution and dendrochronology

The widespread distribution of blue oak across the drainage basins of the Sacramento and San Joaquin (Figure 3a), the principal sources of water for agricultural, industrial, and municipal uses, provided a major motivation for the development of a network of precipitation sensitive blue oak chronologies. Outflow from the Sacramento–San Joaquin delta into San Francisco Bay also influences water quality and habitat conditions in the estuary (Kimmerer 2004). Tree-ring samples were collected from

Figure 2. Ancient blue oak woodlands form the lower forest border between high desert grasslands and the mixed conifer zone along Los Lobos Creek in the Wind Wolves Preserve, a 90 000-acre private conservation property at the southern end of the San Joaquin valley.

36 old-growth blue oak woodlands that roughly span the native distribution of the species (Figure 3b). The point-quarter method of vegetation sampling (Cottam and Curtis 1956; Mitchell 2007) was used to describe the tree species composition at 32 of the blue oak collection sites (Figure 3c). The starting point for a 200-m transect was deliberately sited within an area identified as old-growth blue oak based on the external characteristics of the canopy-dominant trees, including crown dieback, large heavy limbs, dead limbs and branch scars, hollow voids, spiral grain, and exposure of the root collar (Stahle and Chaney 1994). The azimuth of the transect was randomly selected and species composition was measured in four quadrants off the midline of the transect at every 20 m. A random collection of 5-mm-diameter cores was extracted with a Swedish increment borer from the 40 closest blue oak trees in each quadrant [$\geq$10-cm diameter at breast height (DBH)] to characterize the age structure of these stands (Figure 3d). At all locations, old individual trees and relict wood were also sampled in order to maximize the length of the derived tree-ring chronology for climate reconstruction purposes. The collection of randomly sampled cores and deliberately selected cross sections obtained at the Wind Wolves Preserve in Kern County is illustrated in Figure 4.

The interannual variability of blue oak ring widths reflects the history of winter–spring drought and wetness over California (Figure 5). Wet years favor good growth and wide tree rings; drought reduces growth and results in narrow rings. The history of California precipitation is encoded in the time series sequence of wide and narrow rings, and these ring-width patterns can be synchronized among all blue oak in the same woodland and among most oaks in the same region using dendrochronology (Stokes and Smiley 1996). The consistent repetition of the same time series patterns among thousands of living trees confirms the accuracy of this exact chronometer of tree growth and precipitation history.

Dead wood of unknown age can also be dated against the annual ring-width chronology developed from living trees, because distinctive ring-width signatures can be recognized in both living trees and dead wood, fingerprinting their decades
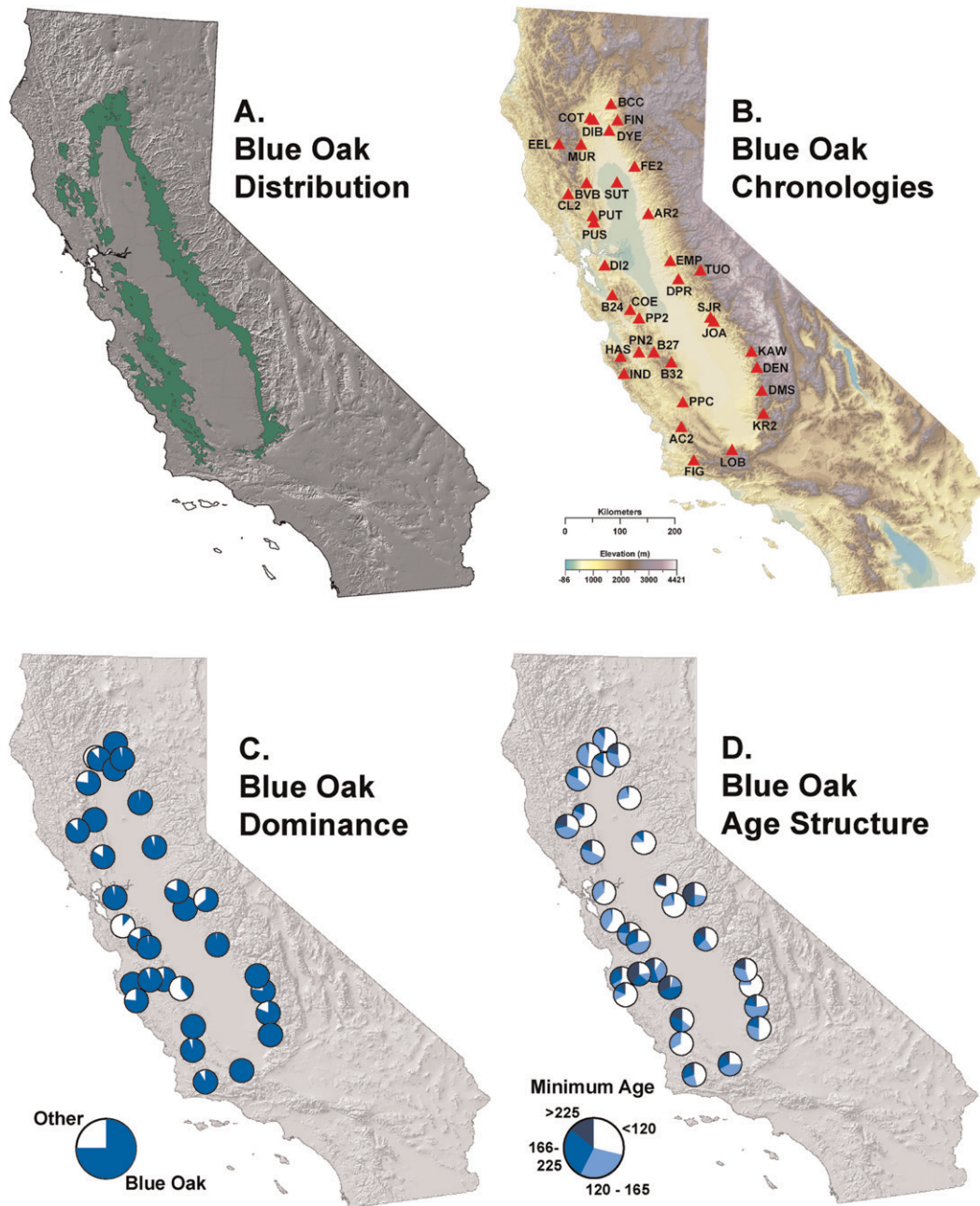
Figure 3. (a) Blue oak is a California endemic species and forms the lower forest border on the foothills that encircle Central Valley (distribution map from Griffin and Critchfield 1972). (b) Tree-ring chronologies were developed for 36 old-growth blue oak woodlands (red triangles). (c) The tree species composition (i.e., blue oak percent of total basal area for all tree species ≥ 10 cm DBH; several sites only contained blue oak) and (d) proportions of blue oak trees at 32 old-growth blue oak stands in four age classes were estimated based on a random sample of 40 trees at each site that were at least 10 cm DBH. Uncut blue oak woodlands with canopy-dominant trees over 200 years old are still widely present throughout its native distribution, especially in the South Coast Ranges and on the rough basalt mesas and slopes of the southern Cascades.

Figure 4. The tree-ring collection from Los Lobos Creek includes core specimens extracted nondestructively from living trees and small radial cross sections cut from fallen logs. The oldest living tree in this sample is at least 377 years old. The oldest dead log has 553 annual rings. The derived tree-ring chronology extends from AD 1333 to 2004.

of contemporaneous growth. The ring-width data recovered from relict wood can be very useful for extending the chronology based on living trees deeper into prehistory. In fact, the earliest years in most of the blue oak chronologies developed during this study are based on exactly cross-dated tree-ring series recovered from dead trees and relict wood that survive in many old-growth blue oak woodlands.

The most important environmental variable controlling the interannual variability of ring width in blue oak near the arid lower forest border is precipitation, accumulated in the soil during the winter and spring seasons (e.g., Kertis et al. 1993; Meko et al. 2011; Stahle et al. 2011). Fortunately, livestock grazing (Mensing 1992), the widespread invasion of nonnative grasses following European settlement (Seabloom et al. 2003), and potential changes in the fire regime (e.g., Swetnam et al. 2009) have not induced a major change in mean growth rate or interannual variability in our sample blue oak chronologies (e.g., see Figure 5 in Stahle et al. 2011). This may be due in part to the extreme climate sensitivity of blue oak growth in the steep, remote, arid lower forest border sites sampled for this analysis (e.g., Figure 5). However, the strength of the precipitation signal in blue oak ring-width chronologies can vary across the ecosystem. Blue oak chronologies developed from the
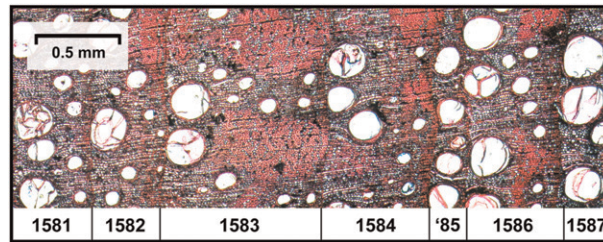
Figure 5. A photomicrograph of the annual rings on a blue oak specimen from Rock Springs Ranch, San Benito County, California (12-μm-thick wafer stained with safranin to enhance lignified structures, in red). Growth proceeded from left to right (1581–87 shown here). Note the large-diameter vessels (white pores) that congregate in the earlywood portion of the annual ring and the dense heavily lignified fiber cells that dominate the latewood (red). The variation in annual ring width can be used as a proxy for water-year precipitation and other hydroclimatic variables in California (e.g., 1583 = wet, 1585 = dry).

most extreme moisture-limited sites tend to be correlated with water-year precipitation, while blue oak found in more mesic conditions at higher elevation or near the northern limits of its range tends to have a weaker response, primarily to spring precipitation. These findings are consistent with classic dendroclimatic theory, first articulated by A. E. Douglass a century ago when he invented tree-ring analysis working with ponderosa pine on the Colorado Plateau and giant sequoia of the Sierra Nevada (e.g., Douglass 1920).

3. Age structure and recruitment history of ancient blue oak woodlands

Tree-ring dating of the age structure of blue oak trees in selected old-growth settings across the species range provides some insight into their recruitment history (Figure 3d). The randomly sampled trees had to be at least 10 cm DBH, so the age of these trees provide an estimate of the recruitment history of the stand and the year when the growing sapling reached breast height, not the true tree age or germination history of the stand. In fact, blue oak seedlings and saplings (<1.5 m in height) can be over 50 years old, so the relationship between recruitment to breast height and the original year of germination may be quite uncertain (Koenig and Knops 2007). In addition, some sample trees suffered varying degrees of heart rot that destroyed the inner rings and made it impossible to determine the exact maximum age of the some trees.

The 1191 randomly selected and dated blue oak trees at all 32 sites averaged 140 years old and just 33.3 cm DBH. Expressed in terms of life expectancy, a blue oak sapling that has survived or "recruited" to breast height has a 50% chance of living for 140 years, a 10% chance of reaching 234 years, and a 1% chance of making 354 years in age (not counting the heavy oak mortality that occurs in the seedling and small sapling stages; Borchert 1990). These age thresholds might reasonably be raised by a decade to allow for heart rot.
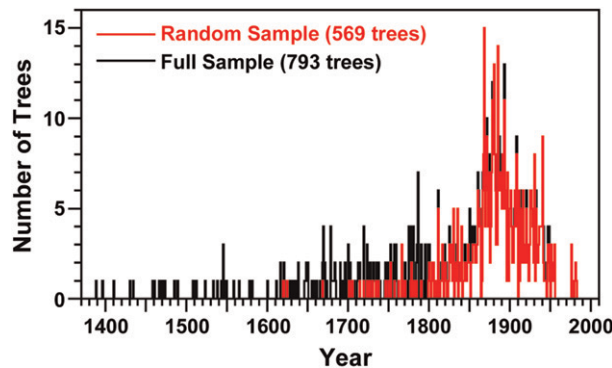
Figure 6. The recruitment dates for a random sample of 569 trees from 32 collection sites that included pith or were near pith are plotted in red, and the pith or near-pith dates for 793 random and selectively sampled trees are plotted in black. A strong peak in blue oak recruitment occurred during the late nineteenth century. These recruitment ages seriously underestimate true germination age (e.g., Koenig and Knops 2007) but are sufficient to prove the great age of many blue oak trees still present in California.

An estimate of the ecosystem-wide recruitment history of blue oak is illustrated in Figure 6 for 569 randomly selected trees that were solid to the center and for all 793 random and selectively sampled trees with complete radii across our 32 study sites (trees lacking the center rings are excluded). Both groups document a major recruitment pulse in the late nineteenth century when millions of seedlings must have reached breast height in the blue oak woodlands of California (as defined here, blue oak seedlings were < 1.5 m tall, saplings were ≥ 1.5 m tall and < 10 cm DBH, and trees were ≥ 10 cm DBH). Depending on the added time necessary for our sample trees to grow from germination to breast height, the 20–30-yr period of peak recruitment might suggest that a highly successful period of germination occurred in the early nineteenth century. When that episode actually was and whether it was truly synchronous across the ecosystem cannot be determined because of the slow and highly variable growth rates for blue oak seedlings. Koenig and Knops (Koenig and Knops 2007) found that blue oak seedlings first measured in 1965 at the Hasting Natural History Reserve were on average only 76.7 cm tall (± 45.0 cm standard deviation) and all were at least 41 years old. How the seedling growing conditions observed by Koenig and Knops (Koenig and Knops 2007) might mimic the browsing pressure and growth rates of blue oak seedlings in the nineteenth century is not known. However, weather and climate variables can synchronize blue oak acorn production at the ecosystem scale (Koenig and Knops 2013), so the blue oak recruitment peak identified in Figure 6 might theoretically echo an earlier period of widespread germination in California. Alternatively, the nineteenth-century peak in recruitment (Figure 6) might only reflect demographic constraints, simply the average life span of tree-sized blue oak, rather than climate or pervasive human impacts.

The decline in recruitment during the twentieth century largely reflects the ≥ 10-cm-DBH sampling threshold. None of the sample blue oak recruited after 1985, and most did not recruit after 1960 (Figure 6). However, some of the late-nineteenth- and

twentieth-century decline in recruitment may also reflect human impacts associated with intensive livestock grazing, invasion of exotic grasses, and altered wildlife and wildfire regimes (White 1966; McCreary 1990; Mensing 1992; Seabloom et al. 2003). This contrasts with the long tail in recruitment before 1850 (Figure 6), which might suggest nearly continuous blue oak recruitment at the landscape level prior to European settlement. Recruitment was more poorly sampled at our 32 individual blue oak stands (not shown), but it was much more episodic and probably reflects the complex result of weather, climate, fire, herbivory, and disease.

The data in Figures 3d and 6 indicate that the old-growth blue oak woodlands sampled in this study are well populated with trees that recruited to tree status in the late nineteenth and early twentieth centuries. However, these stands also preserve an important fraction of trees that recruited before the arrival of the first European settlers (Figure 6, based on minimum age a breast height). The oldest living blue oak tree sampled during this study was at least 459 years old found on Bureau of Land Management property in the mountains north of Coalinga, and many living trees were sampled in the 350–400-yr age class (not counting their potentially significant age at the time of recruitment). Several dead blue oak had over 500 annual rings, and the oldest was a dead tree at Los Lobos with 553 annual rings (dating from AD 1333 to 1884), but this specimen was missing the innermost rings. Based on these results and the age of blue oak seedlings discussed by Koenig and Knops (Koenig and Knops 2007), it is reasonable to conclude that some surviving blue oaks in California are over 600 years old, and a very few select individuals might be over 700 years old. Given the prevalence of heart rot among these most ancient oaks, their true age may never be known. Nevertheless, blue oak is among the oldest angiosperms ever documented with exact tree-ring dating (Brown 2012), and it is reasonable to conclude that thousands of ancient blue oak trees that germinated before Spanish, Mexican, or American settlement still survive across the foothills of the Coast Ranges and Sierra Nevada.

4. The blue oak record of California precipitation

The importance of precipitation to the environmental dynamics of the blue oak ecosystem can be demonstrated by the exceptionally strong and widespread correlations between blue oak tree rings and seasonal precipitation totals. The Mt. Diablo, Rock Springs, and Los Lobos chronologies were each correlated with September–May precipitation totals in the gridded Parameter Elevation Regressions on Independent Slopes Model (PRISM) precipitation dataset (Daly et al. 2008). The strongest correlations with seasonal precipitation ($r \geq 0.90$; $P < 0.001$) were computed with the Mt. Diablo and Rock Springs chronologies, and the spatial correlation pattern of these chronologies covers most of the region that contributes runoff to San Francisco Bay (Figure 7). These broadscale patterns of significant precipitation correlation arise in part from the organized winter storms that deliver most of the annual precipitation across California and Nevada. The outstanding basinwide precipitation history encoded in blue oak ring widths has been used for the reconstruction of winter precipitation (Meko et al. 2011), the soil moisture balance (Cook et al. 2007), Sacramento River streamflow (Meko et al. 2001), and San Francisco Bay salinity (Stahle et al. 2001; Stahle et al. 2011).
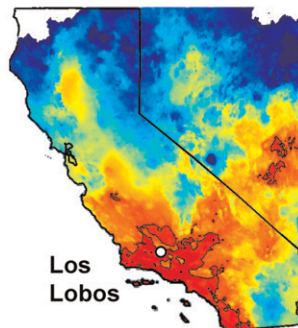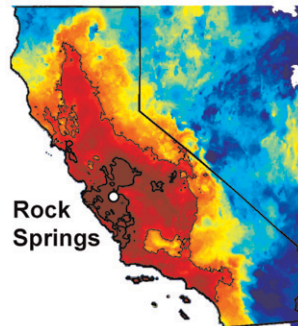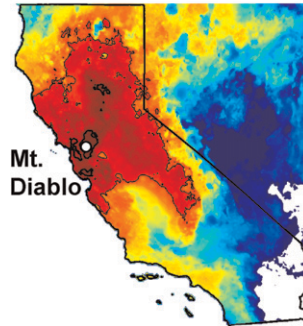
Figure 7. The tree-ring chronologies from Mt. Diablo, Rock Springs, and Los Lobos (white dots) were correlated with the seasonal precipitation totals accumulated from September through May at each grid point in the PRISM precipitation dataset from 1951 to 2003 (Daly et al. 2008). The PRISM data are based on weather station observations that have been distributed across the landscape with a grid spacing of 4 km, taking into account orographic and topographic effects on precipitation. Correlation coefficients computed between these three tree-ring chronologies and the precipitation data at each grid point are contoured and color coded. Red shading indicates correlations above 0.70. Correlations above 0.80 are mapped within the light contour line; correlations above 0.90 are mapped within the heavy line.
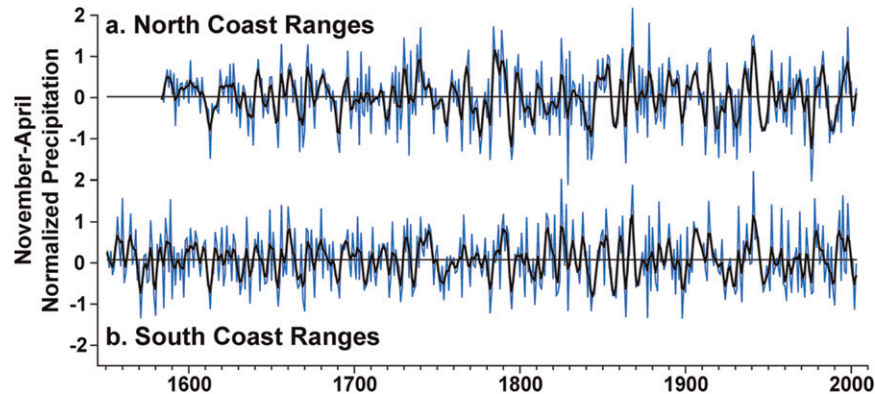
Figure 8. Three site-centered reconstructions were used to compute a regional average of winter precipitation for the (a) North and (b) South Coast Ranges. The site-centered reconstructions from Meko et al. (Meko et al. 2011) for Bear Valley Buttes (BVB), Putah Creek (PUT), and Mt. Diablo (DI2) were used for the North Coast Ranges; reconstructions for Palo Prieto Creek (PPC), Figueroa Mountain (FIG), and Los Lobos Creek (LOB) were used for the South Coast Ranges average (Figure 3b). All six individual reconstructions were well calibrated and verified against instrumental precipitation data (Table 1 of Meko et al. 2011). The annual estimates are plotted in blue and a 5-yr smoothed version is plotted in black (i.e., based on a cubic smoothing spline with a 50% frequency response of 5 years; Cook and Peters 1981).

Meko et al. (Meko et al. 2011) developed "site centered" reconstructions of winter precipitation totals at the 36 blue oak chronology locations (Figure 3b), calibrating the ring-width data with November–April precipitation at the PRISM grid point closest to each tree-ring site. The 36 reconstructions were then used to investigate spatial gradients in precipitation over California for the past 450 years. Here we compute two regional averages of November–April precipitation for the North and South Coast Ranges based on three high-quality site-centered reconstructions in each region (Figure 8) and repeat some of the gradient analyses reported by Meko et al. (Meko et al. 2011). Prior to computing the regional averages, each site-based reconstruction was normalized as

$$\text{normalized } P_t = (P_t - \text{median})(\text{IQR}^{-1}),$$

where P_t is the precipitation total for the November through April season in year t, median is the 50th percentile, and IQR is the interquartile range (i.e., 75th–25th percentiles, computed for the full period available for each reconstruction). The median and IQR were used for normalization because some of the individual reconstructions may not be normally distributed.

The selection of the three site-centered reconstructions in each region attempts to maximize the length of record, strength of the precipitation signal in the tree-ring data (as measured by the calibration and verification statistics; Table 1 of Meko

et al. 2011), and their location to emphasize the latitudinal differences in cool season precipitation over California. The North Coast Ranges precipitation reconstruction is highly correlated with winter precipitation over central and Northern California, particularly over the drainage basin of the Sacramento River (Figure 9a). The reconstruction for the South Coast Ranges is most strongly correlated with winter precipitation over central and Southern California, including the southern Sierra Nevada and the drainage basin of the San Joaquin River (Figure 9b). Many drought extremes are reconstructed in both the North and South Coast Ranges, including in 1782, 1795, 1829, 1864, and 1898 during the historical period when documentary or early instrumental observations provide confirmation of widespread dryness over California (e.g., Brewer 1930; Rowntree 1985; CDWR 2012; Figure 8). Several wetness extremes are also reconstructed simultaneously in the North and South Coast Ranges, including 1862, 1868, and 1878 when extreme flooding occurred on the Sacramento River and helped stimulate major water management initiatives in California (Kelly 1989; Figure 8).

The North and South Coast Ranges precipitation reconstructions are intercorrelated for the common period 1584–2003 ($r = 0.64$ for the annual values and $r = 0.65$ for the 5-yr smoothed values; Figure 8), as are the two regional averages of instrumental winter precipitation data based on the same three PRISM grid points in each region ($r = 077$; 1896–2003; not shown). However, there are notable episodes when reconstructed precipitation amounts were different between the North and South Coast Ranges (e.g., 1770s, 1810s–40s, 1970s; Figure 8). An index of the gradient in winter precipitation anomalies that occasionally develop between Northern and Southern California was computed as the simple difference between normalized winter precipitation (November–April) for the North and South Coast Ranges, using both the reconstructed and instrumental data in each region (Figure 10a). This "north–south index" is positively correlated with winter precipitation over the Pacific Northwest but is negatively correlated over Southern California, highlighting the north–south gradient in winter precipitation that occasionally develops over the West Coast (Figure 9c). Strong positive anomalies in the index represent winters that were wetter toward Northern California and strong negative anomalies indicate winters that were wetter toward Southern California (Figures 10a,b). Near-normal index values represent similar winter precipitation conditions over both Northern and Southern California (i.e., no sharp precipitation gradient). The reconstructed gradient index is correlated with the instrumental gradient at $r = 0.78$ for the common period 1896–2003 (Figure 10a).

Extremes in the observed and tree-ring reconstructed precipitation gradient between the North and South Coast Ranges (Figures 10a,b) appear to often represent anomalies in the latitudinal position of the mean storm track and landfalling atmospheric rivers during the cool season (Cayan 1996; Dettinger and Ralph 2011). Landfall as far south as northern Baja California has been associated with atmospheric-river contribution to heavy precipitation events in the interior southwestern United States (Rutz and Steenburgh 2012). Composite analyses of the 500-mb geopotential height field during the most extreme positive and negative years in the instrumental north–south index indicate major circulation changes over the North Pacific and North America between these latitudinal precipitation extremes (Figure 11a,c). During the positive extremes a strong blocking ridge is present near Greenland, coupled with below-normal heights over the Pacific Northwest and
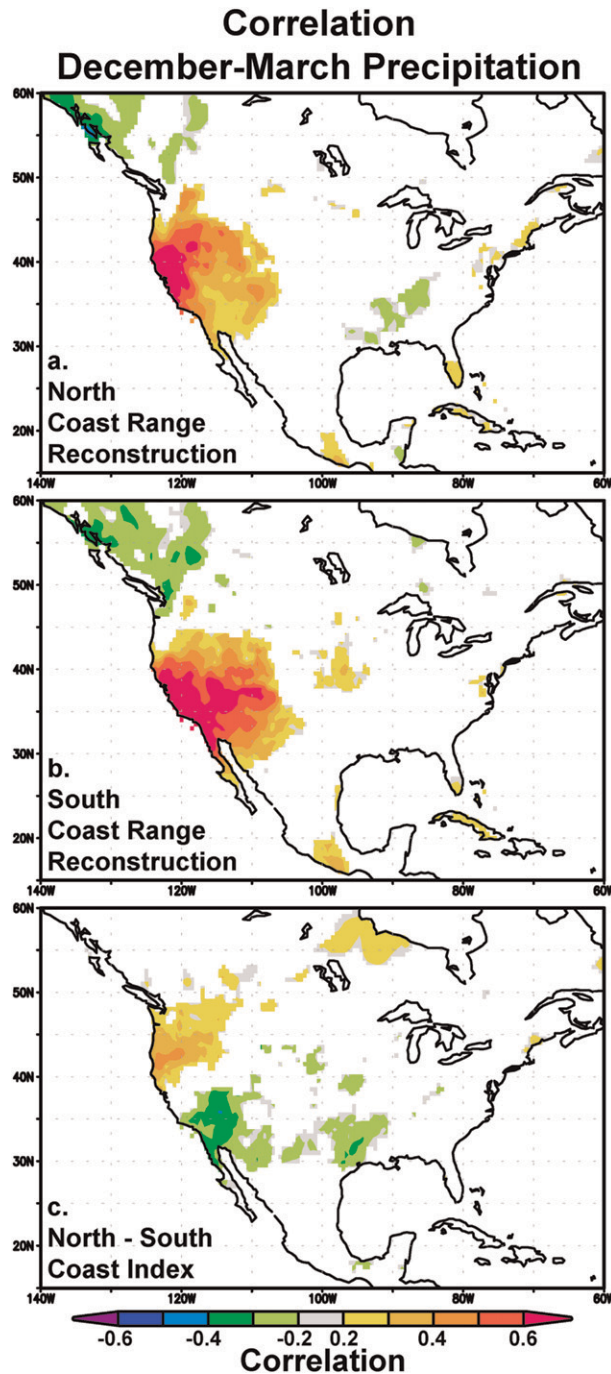
Figure 9. Reconstructed winter precipitation for the (a) North and (b) South Coast Ranges is correlated with December–March precipitation totals. (c) The north–south index is correlated with gridded December–March precipitation. Correlations are mapped using the Royal Netherlands Meteorological Institute (KNMI) Climate Explorer (Trouet and van Oldenborgh 2013) applied to 0.5° Climatic Research Unit (CRU) Ts3.10.01 gridded precipitation for 1901–2002 (Harris et al. 2013). Correlations significant at the 0.1 level are colored.
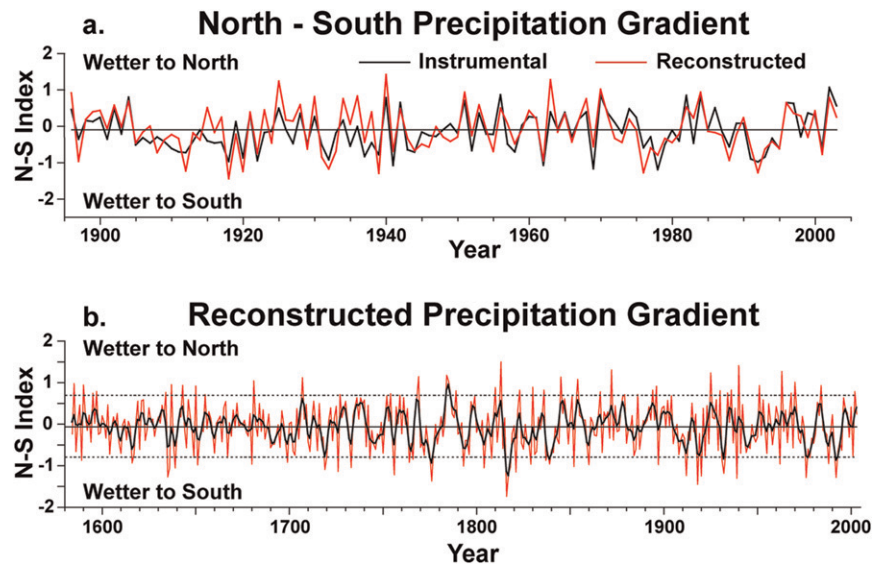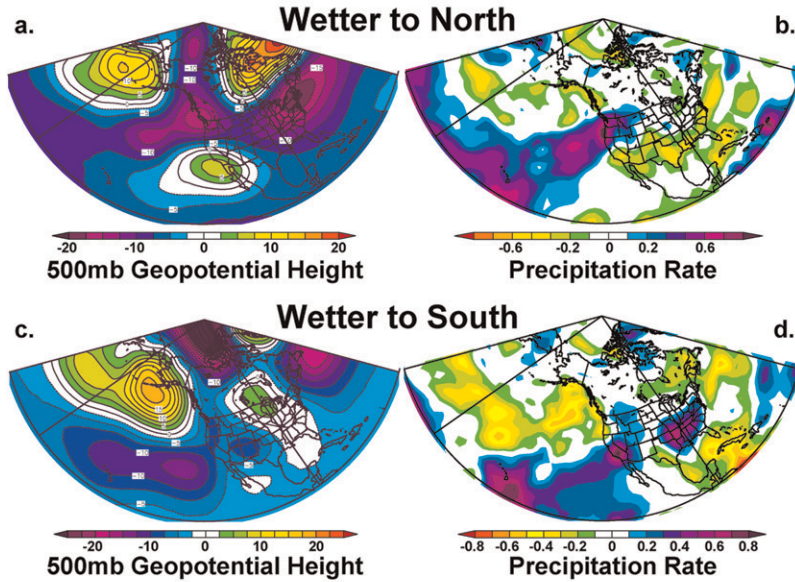
Figure 10. An index of the gradient in precipitation anomalies sometimes present over California was computed between the North and South Coast Ranges reconstructions (i.e., north–south index), where strong positive departures indicate relatively wetter conditions toward Northern California and negative indices indicate wetter conditions toward Southern California. (a) The instrumental and reconstructed indices are plotted from 1896 to 2003 and (b) the reconstructed index is presented from 1584 to 2003 along with the 90th and 10th percentiles and a 5-yr smoothed version. The instrumental and reconstructed indices are correlated at $r = 0.78$ (1896–2003).

above-normal heights off of Southern California (i.e., Northern California wet; Figure 11a). A steep pressure gradient is present over Northern California and Oregon, where it would favor moisture advection and precipitation, as indicated in the composite map of precipitation rate for the same 10 positive index extremes (Figure 11b).

The 500-mb pattern changes sharply for the 10 most negative extremes in the instrumental north–south index (i.e., Southern California wet; Figure 11c), with above-normal heights over the Gulf of Alaska and below-normal heights off Southern California. The composite map of precipitation rate during these negative instrumental extremes confirms the anomalously wet conditions over Southern California (Figure 11d). Note also that the composite precipitation rates both indicate a corridor connecting positive precipitation over Northern (Figure 11b) and Southern California (Figure 11d) with tropical precipitation rates in the central Pacific that may reflect the mean position of atmospheric rivers delivering much of the moisture to California during these regimes. The 500-mb circulation and precipitation rate maps composited during the 20 most positive and 20 most negative reconstructed north–south indices are similar to those illustrated for the instrumental index but tend to be weaker (Figures 11e–h).

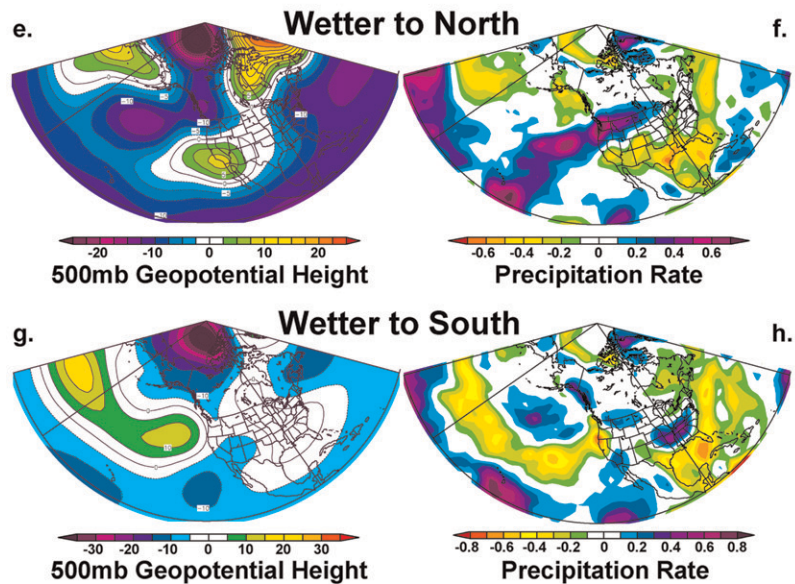# Instrumental N-S Index Extremes (10)

Figure 11. Composite maps of (a),(c) 500-mb geopotential height and (b),(d) precipitation rate over the Pacific–North America (PNA) sector during the 10 most positive and 10 most negative extremes of the instrumental north–south index from 1896 to 2005 are plotted (i.e., Northern California wet and Southern California wet, respectively). (e)–(h) The same variables are plotted for the 20 most extreme positive and negative reconstructed north–south indices from 1871 to 2003. The instrumental height and precipitation rate values were obtained from the Twentieth Century Reanalysis fields and the maps were computed and plotted using the online tools available from the National Oceanic and Atmospheric Administration (NOAA)/Earth System Research Laboratory (http://www.esrl.noaa.gov/psd/data/20thC_Rean/).

The *North American Drought Atlas* (*NADA*; Cook et al. 2007; Cook et al. 2010) was used to map the tree-ring reconstructed soil moisture conditions for the years when the reconstructed north–south index was above the 95th percentile (Figure 12a) and below the 5th percentile from 1584 to 1990 (Figure 12b). These maps support an association between extremes of the north–south index and the longitudinal precipitation gradient and indicate that the blue oak reconstructions reflect in part very-large-scale anomalies in precipitation over western North America. The composite Palmer drought severity index (PDSI) anomalies were more extreme for negative north–south indices when the winter precipitation gradient was wetter toward Southern California (Figure 12b), perhaps due in part to better registration of drought years in the available tree-ring data from Northern California and the Pacific Northwest.

The difference index between reconstructed winter precipitation in Northern and Southern California highlights some interesting individual years and decade-long regimes when there was a strong north–south cool seasonal precipitation gradient across California (Figure 10b). The most anomalous negative differences are reconstructed for 1816–17 in the aftermath of the cataclysmic volcanic eruption of Tambora in Indonesia when the southwestern United States and northern Mexico were extraordinarily wet while the Pacific Northwest was dry (Meko et al. 2011). In fact, the period from 1814 to 1845 seems to have been dominated by relatively moist conditions to the south coincident with drier than normal conditions to the north (Figure 10b). Similar regimes of relative dryness in the north and wetness in the south are reconstructed during the 1770s and 1920s and during portions of the 1970s, 1980s, and 1990s. These spatial anomalies are interesting from a water supply perspective because some 75% of the surface water resources in the state are obtained from Northern California (CDWR 2012).

5. Reconstructed San Francisco Bay salinity for the past 670 years

San Francisco Bay is one of the most altered estuaries in the world (Nichols et al. 1986) and is now the target of intensive management and restoration efforts by state and federal agencies (Kimmerer et al. 2005). Salinity in the estuary is controlled primarily by freshwater discharged from the Sacramento and San Joaquin Rivers and by winds, tides, and the coastal ocean (Peterson et al. 1995). The instrumental record of near-surface salinity in San Francisco Bay was long monitored at Ft. Point near the Golden Gate. The Ft. Point observations began in 1922 and the station was abandoned in 1994. Prior to 1952 the seasonal salinity data at Ft. Point primarily reflect natural hydroclimatic variability, but after 1952 they are increasingly biased by anthropogenic diversion of Sacramento and San Joaquin streamflow. Blue oak chronologies are highly correlated with seasonal precipitation and runoff totals and as a result are also correlated with seasonal salinity levels in the estuary.

A regional average tree-ring chronology based on three selected blue oak sites (Mt. Diablo, Rock Springs Ranch, and Los Lobos) was used to calibrate the early Ft. Point salinity record and to estimate the natural precipitation-driven variability in seasonal salinity levels in the present and preceding centuries (Figure 13, updating

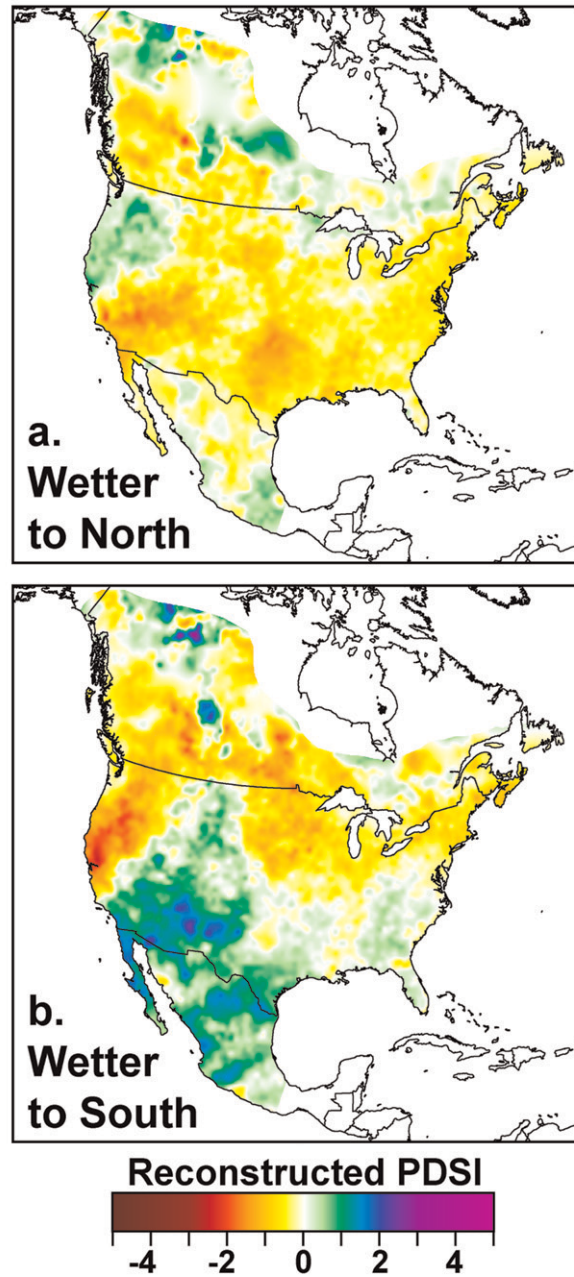## North American Drought Atlas

Figure 12. Composite maps of the tree-ring reconstructed PDSI are plotted for years when the reconstructed north–south index for California (Figure 10b) was (a) above the 95th and (b) below the 5th percentiles (21 years each). The PDSI reconstructions were obtained from the North American Drought Atlas (Cook et al. 2007; Cook et al. 2010; Cook and Krusic 2013) and are influenced by moisture conditions during and preceding the growing season (Cook et al. 1999).
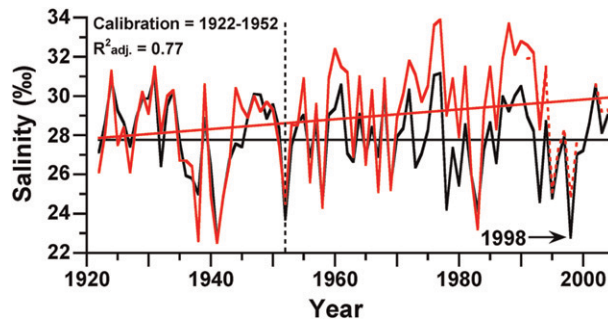
Figure 13. Observed and tree-ring reconstructed January–July near-surface salinity at Ft. Point near the Golden Gate, 1922–2005 (red and black curves, respectively). The Ft. Point record ended in 1994 and has been extended to 2005 based on regression estimates from salinity observations made at Point San Pablo (dashed line; with missing values; Buchanan 2007). The impact of drought and freshwater diversion are indicated by the high salinity measurements from the 1960s to the early 1990s (note the positive linear trend fit to the observed data from 1922 to 2005 in red), particularly when compared with the tree-ring estimates based on precipitation/streamflow forcing (black time series). The bay was freshened during the high runoff regime of the late 1990s.

and extending an earlier reconstruction by Stahle et al. 2001). The blue oak reconstruction of estuarine salinity was calibrated with the Ft. Point data from 1922 to 1952, prior to heavy freshwater diversions from the delta [a few missing monthly observations were replaced with estimates from an estuarine salinity model (Knowles 2002); the Ft. Point record ended in 1994 and has been extended to 2005 based on estimates from Point San Pablo (Figure 13)].

The strong statistical association between the instrumental and tree-ring reconstructed salinity data for the January–June season is illustrated in Figure 13 for the 1922–52 calibration period [$R^2 = 0.77$ (adjusted for the loss of one degree of freedom); Durbin–Watson statistic $= 2.12$ (indicating no significant autocorrelation in the regression residuals)]. The Ft. Point salinity data become increasingly impacted by water use and diversion in the middle to late twentieth century, and these anthropogenic changes are reflected in the verification statistics calculated between the observed and reconstructed salinity data for 1953–99. The reconstructed data are well correlated with the actual salinity data ($r = 0.82$; 1953–99), but the lower reduction of error (RE $= 0.43$) and coefficient of efficiency (CE $= 0.25$) statistics, compared with the explained variance in the calibration period ($R^2 = 0.77$), both indicate that the reconstruction does not track the persistent changes in the mean of the instrumental record during the verification period (Figure 13).

San Francisco Bay salinity levels rose on average from the 1950s to the mid-1990s, peaking during the historic droughts of 1976–77 and 1987–92 (Figure 13). These were extraordinary droughts but estuarine salinity levels appear to have been made unnaturally high by freshwater diversion from the Sacramento and San Joaquin Rivers. The tree-ring reconstruction suggests that the salinity levels recorded at Ft. Point during these late-twentieth-century droughts were not matched over the
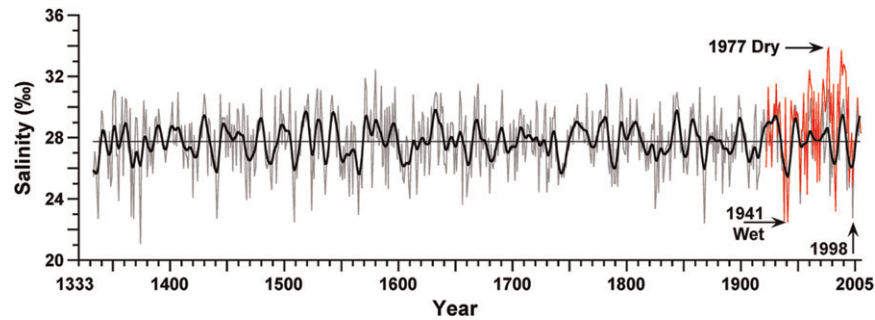
Figure 14. The blue oak reconstruction of January–July average near-surface sa-linity at Ft. Point is illustrated from 1333 to 2005 (gray curve; decadal variability highlighted with the black curve; note that drought and high salinity excursions are indicated above the mean, the opposite of low precipitation amounts in Figure 8). The observed salinity values mea-sured at Ft. Point from 1922 to 2005 are shown in red. Note the high salinity extremes during the period of heavy streamflow diversion after World War II. High salinity extremes occur during drought, and the extremes witnessed during the 1976, 1977, 1988, and 1990 droughts have not been matched over the past 673 years. Low salinity extremes occur during wet years, including several El Niño events (e.g., 1868, 1941, 1983, and 1998). The tree-ring data suggest that salinity during the 1998 El Niño event should have been among the lowest seasonal averages in the past 673 years.

past 673 years (Figure 14). Alternatively, the freshest season-long conditions in the estuary have tended to occur during heavy winter precipitation and runoff regimes associated with El Niño events (e.g., 1868, 1940/41, 1982/83, and 1997/98; Figures 13 and 14).

The salinity balance in San Francisco Bay has improved after the drought of 1987–92. Since that time, increased precipitation and runoff led to seasonal salinity averages more in line with that expected based on seasonal precipitation totals as estimated via blue oak tree-ring chronologies (Figure 13). However, the tree-ring reconstruction suggests that during the strong El Niño event of 1998 seasonal salinity was not as low as expected based on precipitation, runoff, and blue oak growth (Figure 13), which given the amount of blue oak growth in that remarkable year should have been one of the lowest estuarine salinity averages in the past 673 years (Figure 14).

Drought during the 1920s and 1930s resulted in persistently high salinity levels in San Francisco Bay (Figure 13). In fact, the reconstruction suggests that the 1920–30s suffered one of the most severe and sustained drought/high salinity episodes of the past 673 years (Figure 14). Other salinity maxima nearly 20 years long were re-constructed during droughts of the late sixteenth, late eighteenth, and early nineteenth centuries. By comparison, the disruptive drought and high salinity episode from 1987 to 1992 was relatively brief (based on the tree-ring reconstruction, Figures 13 and 14), and the recurrence of more persistent drought as witnessed in this reconstruction would pose a serious challenge to the management of water and ecosystem function in California.

Figure 15. San Luis Reservoir in Merced County stores Sacramento–San Joaquin water diverted from the delta and bound for Southern California. The blue oak trees shown here at Pacheco State Park and elsewhere provide long precipitation proxies that can contribute to the understanding and management of these vital water supplies.

6. Conclusions

Centuries-old blue oak trees are especially abundant on the foothills at Pacheco Pass above San Luis Reservoir (Figure 15). Ironically, San Luis Reservoir is located in the arid rain shadow of the Diablo Range and impounds ephemeral drainages that are, by themselves, inadequate to provide sufficient runoff to fill this large impoundment. Most of the water in San Luis Reservoir has been imported from the Sacramento and San Joaquin delta and is stored for transfer to Southern California. The climate variations that modify Sacramento–San Joaquin runoff and ultimately dictate the volume of water available for agricultural, industrial, and municipal consumption are encoded in the thickness of annual rings in ancient blue oak at Pacheco Pass and elsewhere in California. The new network of 36 blue oak chronologies also preserves a long-term spatial record of atmospheric circulation and the atmospheric rivers that deliver much of the vital winter moisture to California.

The precise location and size of ancient blue oak forest remnants need to be identified and mapped in order to direct conservation efforts to the areas with highest ecological integrity. We have identified several large tracts of ancient blue oak in the Lassen, Sierra, Sequoia, and Los Padres National Forests and on Bureau of Land Management property in the South Coast Ranges. California state parks, the Nature Conservancy, and Wind Wolves Preserve have also conserved spectacular landscapes with ancient blue oak. However, most of the blue oak ecosystem is located on private property so the efforts of the California Oak Foundation and the California Wildlife Foundation (http://www.californiaoaks.org/) to promote the sustainable management of oak woodlands are vital to the future of these woodlands. The remarkable history of precipitation, streamflow, and estuarine water quality embedded in the annual rings of ancient blue oak trees may add some further justification to the conservation of this beautiful California ecosystem (Figure 16).

Figure 16. This 350-yr-old blue oak is located near the north fork of the Kaweah River in Sequoia National Park. In a state and national park famous for magnificent trees, the remaining blue oak woodlands of California are remarkable for their abundance, longevity, and environmental history encoded in their annual growth rings.

References

Borchert, M., 1990: From acorn to seedling: A perilous stage. *Fremontia,* **18,** 36–37.

Brewer, W. H., 1930: *Up and Down California in 1860-1864; The Journal of William H. Brewer.* 1st ed. Yale University Press, 601 pp.

Brown, P. M., cited 2012: OldList. [Available online at http://www.rmtrr.org/oldlist.htm.]

Buchanan, P. A., 2007: Specific conductance and water temperature data, San Francisco Bay, California, for water year 2005. *Interagency Ecological Program Newsletter,* Vol. 20, No. 2, California Department of Water Resources, Sacramento, CA, 60–63.

Cayan, D. R., 1996: Interanual climate variability and snowpack in the western United States. *J. Climate,* **9,** 928–948.

CDWR, 2012: Drought in California. California Department of Water Resources Rep., 12 pp. [Available online at http://www.water.ca.gov/waterconditions/drought/docs/Drought2012.pdf.]

Cook, E. R., and K. Peters, 1981: The smoothing spline: A new approach to standardizing forest interior tree-ring series for dendroclimatic studies. *Tree-Ring Bull.,* **41,** 45–53.

——, and P. J. Krusic, cited 2013: North American Drought Atlas. Lamont-Doherty Earth Observatory. [Available online at http://iridl.ldeo.columbia.edu/SOURCES/.LDEO/.TRL/.NADA2004/.pdsi-atlas.html.]

——, D. M. Meko, D. W. Stahle, and M. K. Cleaveland, 1999: Drought reconstructions for the continental United States. *J. Climate,* **12,** 1145–1162.

——, R. Seager, M. A. Cane, and D. W. Stahle, 2007: North American drought: Reconstructions, causes, and consequences. *Earth Sci. Rev.,* **81,** 93–134.

——, ——, R. R. Heim, R. S. Vose, C. Herweijer, and C. W. Woodhouse, 2010: Megadroughts in North America: Placing IPCC projections of hydroclimatic change in a long-term paleoclimate context. *J. Quat. Sci.,* **25,** 48–61.

Cottam, G., and J. T. Curtis, 1956: The use of distance measures in phytosociological sampling. *Ecology,* **37,** 451–460.

Daly, C., M. Halbleib, J. I. Smith, W. P. Gibson, M. K. Doggett, G. H. Taylor, J. Curtis, and P. A. Pasteris, 2008: Physiographically sensitive mapping of temperature and precipitation across the conterminous United States. *Int. J. Climatol.,* **28,** 2031–2064, doi:10.1002/joc.1688.

Dettinger, M. D., and F. M. Ralph, 2011: Storms, floods, and the science of atmospheric rivers. *Eos, Trans. Amer. Geophys. Union,* **92,** 265–266.

Douglass, A. E., 1920: Evidence of climatic effects in the annual rings of trees. *Ecology,* **1,** 24–32.

Griffin, J. R., and W. E. Critchfield, 1972: The distribution of forest trees in California. USDA Forest Service Res. Paper PSW-82, 60 pp.

——, and P. C. Muick, 1990: California native oaks: Past and present. *Fremontia,* **18,** 4–12.

Harris, I., P. D. Jones, T. J. Osborn, and D. H. Lister, 2013: Updated high-resolution grids of monthly climatic observations—The CRU TS3.10 dataset. *Int. J. Climatol.,* in press.

Kelly, R. L., 1989: *Battling the Inland Sea: Floods, Public Policy, and the Sacramento Valley.* University of California Press, 395 pp.

Kertis, J. A., R. Gross, D. L. Peterson, M. J. Arbaugh, R. B. Standiford, and D. D. McCreary, 1993: Growth trends of blue oak (*Quercus douglasii*) in California. *Can. J. For. Res.,* **23,** 1720–1724.

Kimmerer, W., 2004: Open water processes of the San Francisco Estuary: From physical forcing to biological responses. San Francisco Estuary and Watershed Science Rep., 142 pp. [Available online at http://www.escholarship.org/uc/item/9bp499mv.]

——, D. D. Murphy, and P. L. Angermeier, 2005: A landscape-level model for ecosystem restoration in the San Francisco estuary and its watershed. San Francisco Estuary and Watershed Science Rep., 19 pp.

Knowles, N., 2002: Natural and management influences on freshwater inflows and salinity in the San Francisco estuary at monthly to interannual scales. *Water Resour. Res.,* **38,** 1289, doi:10.1029/2001WR000360.

Koenig, W. D., and J. M. H. Knops, 2007: Long-term growth and persistence of blue oak (*Quercus douglasii*) seedlings in a California oak savanna. *Madrono,* **54,** 269–274.

——, and ——, 2013: Large-scale spatial synchrony and cross-synchrony in acorn production by two California oaks. *Ecology,* **94,** 83–93.

McCreary, D. D., 1990: Native oaks—The next generation. *Fremontia,* **18,** 44–47.

Meko, D. M., M. D. Therrell, C. H. Baisan, and M. K. Hughes, 2001: Sacramento River flow reconstructed to A.D. 869 from tree rings. *J. Amer. Water Resour. Assoc.,* **37,** 1029–1039.

——, D. W. Stahle, D. Griffin, and T. A. Knight, 2011: Inferring precipitation-anomaly gradients from tree rings. *Quat. Int.,* **235,** 89–100.

Mensing, S. A., 1992: The impact of European settlement on blue oak (*Quercus douglasii*) regeneration and recruitment in the Tehachapi Mountains, California. *Madrono,* **39,** 36–46.

Mitchell, K., 2007: Quantitative analysis by the point-centered quarter method. Hobart and William Smith Colleges Rep., 34 pp. [Available online at http://people.hws.edu/mitchell/PCQM.pdf.]

Nichols, F. H., J. E. Cloern, S. N. Louma, and D. H. Peterson, 1986: The modification of an estuary. *Science,* **231,** 567–573.

Pavlik, B. M., M. C. Muick, S. G. Johnson, and M. Popper, 1991: *The Oaks of California.* Cachima Press, 184 pp.

Peterson, D. H., D. R. Cayan, J. DiLeo, M. A. Noble, and M. D. Dettinger, 1995: The role of climate in estuarine variability. *Amer. Sci.,* **83,** 58–67.

Rowntree, L. B., 1985: Drought during California's mission period, 1769-1834. *J. Calif. Great Basin Anthropol.,* **7,** 7–20.

Rutz, J. J., and W. J. Steenburgh, 2012: Quantifying the role of atmospheric rivers in the interior western United States. *Atmos. Sci. Lett.,* **13,** 257–261.

Seabloom, E. W., W. S. Harpole, O. J. Reichman, and D. Tilman, 2003: Invasion, competitive dominance, and resource use by exotic and native California grassland species. *Proc. Natl. Acad. Sci. USA,* **100,** 13 384–13 389.

Stahle, D. W., and P. L. Chaney, 1994: A predictive model for the location of ancient forests. *Nat. Areas J.,* **14,** 151–158.

——, M. D. Therrell, M. K. Cleaveland, D. R. Cayan, M. D. Dettinger, and N. Knowles, 2001: Ancient blue oak reveal human impact on San Francisco Bay salinity. *Eos, Trans. Amer. Geophys. Union,* **82,** 141–145.

——, and Coauthors, 2011: A tree-ring reconstruction of the salinity gradient in the northern estuary of San Francisco Bay. San Francisco Estuary and Watershed Science Rep. 9-1, 22 pp. [Available online at http://www.escholarship.org/uc/item/5cz3q8v4.]

Stokes, M. A., and T. L. Smiley, 1996: *An Introduction to Tree-Ring Dating.* University of Arizona Press, 73 pp.

Swetnam, T. W., C. H. Baisan, A. C. Caprio, P. M. Brown, R. Touchan, R. S. Anderson, and D. J. Hallett, 2009: Multi-millennial fire history of the Giant Forest, Sequoia National Park, California, USA. *Fire Ecol.,* **5,** 120–150.

Trouet, V., and G. J. van Oldenborgh, 2013: KNMI Climate Explorer: A web-based research tool for high-resolution paleoclimatology. *Tree-Ring Res.,* **69,** 3–13.

White, K. L., 1966: Structure and composition of foothill woodland in central coastal California. *Ecology,* **47,** 229–237.